PROCEEDINGS OF SCIENCE

Four-dimensional QCD equation of state at finite chemical potentials

Akihiko Monnai,[a,*] **Grégoire Pihan,**[b] **Björn Schenke**[c] **and Chun Shen**[d]

[a] *Department of General Education, Faculty of Engineering, Osaka Institute of Technology, Osaka 535-8585, Japan*

[b] *Physics Department, University of Houston, Houston, Texas 77004, USA*

[c] *Physics Department, Brookhaven National Laboratory, Upton, NY 11973, USA*

[d] *Department of Physics and Astronomy, Wayne State University, Detroit, Michigan 48201, USA*

E-mail: akihiko.monnai@oit.ac.jp

Exploration of the QCD phase diagram is pivotal in particle and nuclear physics. We construct a full four-dimensional equation of state of QCD with net baryon, electric charge, and strangeness by extending the NEOS model beyond the conventional two-dimensional approximation. Lattice QCD calculations based on the Taylor expansion method and the hadron resonance gas model are considered for the construction. We also develop an efficient numerical method for applying the four-dimensional equation of state to relativistic hydrodynamic simulations, which can be used for the analysis of nuclear collisions at beam energy scan energies and for different nuclear species at the BNL Relativistic Heavy Ion Collider.

The XVIth Quark Confinement and the Hadron Spectrum Conference (QCHSC24)
19-24 August, 2024
Cairns Convention Centre, Cairns, Queensland, Australia

*Speaker

 ISSN 1824-8039 . Published by SISSA Medialab.

PoS(QCHSC24)163

1. Introduction

Nuclear matter under extreme conditions has been a topic of significant interest. First-principles calculations based on the lattice QCD method indicate that quarks and gluons are deconfined from hadrons to form the quark-gluon plasma (QGP) at high temperatures above 155-160 MeV [1–3]. Nuclear collisions at the BNL Relativistic Heavy Ion Collider (RHIC) and the CERN Large Hadron Collider (LHC) can experimentally produce the QGP, providing unique opportunities to explore the dynamical evolution and statistical properties of the QCD system at various energies with different colliding nuclei. The beam energy scan (BES) program at RHIC is devoted to the exploration of the QCD phase diagram [4].

A major discovery in high-energy nuclear collisions is that the QGP exhibits near-perfect fluidity [5, 6]. The relativistic hydrodynamic model with hadronic afterburner and realistic initial conditions has been successful in describing the centrality, collision energy, and momentum dependencies of hadronic yields. It has been established as a unique tool for describing the strongly coupled QCD system dynamically near the quark-hadron crossover temperature, where first-principles methods face difficulties. The model is supplemented with the equation of state, in which the thermodynamic properties of the system are encoded.

One of the goals of QCD phenomenology is to elucidate the QCD equation of state at finite densities [7–16]. In this study, we develop a lattice-QCD-based model for the equation of state with multiple conserved charges: net baryon (B), electric charge (Q), and strangeness (S) [10, 11, 13, 17–20]. The hadron resonance gas model, which can reproduce lattice QCD results at zero chemical potentials, is employed as a description of the low-temperature regime. Such models can be found in Refs. [10, 11] as functions of temperature and chemical potentials, but they have not been fully formulated as functions of energy and conserved charge densities, which appear in the hydrodynamic equations of motion. We introduce novel variables that enable evolution of multiple conserved currents and efficient numerical simulations of relativistic nuclear collisions [21, 22]. An alternative approach can be found in Refs. [15, 23].

2. The equation of state

The hybrid QCD equation of state model, NEOS-4D, is constructed based on the Taylor expansion method [24, 25] of lattice QCD simulations:

$$\frac{P_{\rm lat}}{T^4} = \frac{P_0}{T^4} + \sum_{l,m,n} \frac{\chi^{B,Q,S}_{l,m,n}}{l!m!n!} \left(\frac{\mu_B}{T}\right)^l \left(\frac{\mu_Q}{T}\right)^m \left(\frac{\mu_S}{T}\right)^n. \tag{1}$$

P_0 and $\chi^{B,Q,S}_{l,m,n}$ are the pressure and susceptibilities defined at vanishing chemical potentials. We use all susceptibilities up to the fourth order from lattice QCD simulations [2, 26–29] and parametrize χ^B_6, χ^{BQ}_{51}, and χ^{QS}_{51} as defined in Ref. [10] for thermodynamic consistency. The pressure is smoothly connected to that of the hadron resonance gas model around the quark-hadron crossover because the expansion method is not convergent at large fugacities [30]:

$$P = \frac{1}{2}\left(1 - \tanh\frac{T-T_c}{\Delta T_c}\right)P_{\rm had} + \frac{1}{2}\left(1 + \tanh\frac{T-T_c}{\Delta T_c}\right)P_{\rm lat}. \tag{2}$$

This yields a crossover equation of state. $T_c(\mu_B) = a - d(b\mu_B^2 + c\mu_B^4)$ is the connection temperature and $\Delta T_c = 0.1T_c(0)$ is the width of the connection region. We use $a = 0.16$ GeV, $b = 0.139$ GeV^{-1}, $c = 0.053$ GeV^{-3}, and $d = 0.4$ motivated by the chemical freezeout [31]. The hadronic pressure is

$$P_{\rm had} = \pm T \sum_i \int \frac{g_i d^3 p}{(2\pi)^3} \ln[1 \pm e^{-(E_i - \mu_i)/T}], \tag{3}$$

where the index i denotes hadronic particle species. We consider the hadrons and resonances lighter than 2 GeV that have u, d, or s as valence quarks from the particle data group [32]. g_i is the degeneracy and μ_i is the hadronic chemical potential. The positive sign is for baryons and the negative sign is for mesons. Other thermodynamic variables, such as e, s, n_B, n_Q, n_S, and c_s, can be obtained through the fundamental thermodynamic relations.

3. Numerical results

We estimate the four-dimensional equation of state in numerical simulations. Dimensionless pressure P/T^4 as a function of μ_B, μ_Q, and μ_S is shown at different T in the vicinity of the QCD crossover in Fig. 1. One can see that the pressure tends to become large at larger temperatures and chemical potentials. It is intrinsically symmetric under the simultaneous sign conversion of μ_B, μ_Q, and μ_S. On the other hand, the pressure is asymmetric under the sign conversion of a single chemical potential because off-diagonal susceptibilities mix the contributions of different chemical potentials. Figure 2 shows the dependence of P/T^4 on each chemical potential. It is most sensitive to μ_Q and least to μ_B in the hadronic phase because the lightest carriers of electric, strangeness, and baryon charges are pions, kaons, and protons, respectively. On the other hand, in the parton gas limit P/T^4 is most sensitive to μ_S and least to μ_B because the lowest-order diagonal susceptibilities approach $\chi_2^S = 1$, $\chi_2^Q = 2/3$, and $\chi_2^B = 1/3$ (see also Eqs.(5)-(7) for references).

The entropy-to-baryon density ratio s/n_B remains unchanged during ideal hydrodynamic evolution in nuclear collisions. Therefore, the constant s/n_B lines can characterize the region in the phase diagram explored at each collision energy [33]. The trajectories are also affected by n_Q and n_S. Here, we consider $n_Q/n_B = 0$ and $n_Q/n_B = 1$ as limiting cases corresponding to neutron-rich and proton-rich domains of the initial geometry in nuclear collisions, respectively, and the strangeness neutrality condition $n_S = 0$ for demonstration. It should be noted that these conditions can be modified in the presence of additional fluctuation or dissipation.

Figure 3 shows the trajectories of $s/n_B = 420, 144, 51$ and 30, which represent the collider energies of $\sqrt{s_{\rm NN}} = 200, 62.4, 19.6$ and 14.5 GeV, respectively, in the (a) T-μ_B, (b) T-μ_Q, and (c) T-μ_S planes, where the other chemical potentials are set to zero. The bands illustrate the range between the $n_Q/n_B = 0$ and $n_Q/n_B = 1$ cases. The thick lines in the middle of the bands denote the average case $n_Q/n_B = 0.4$ that is implied by the Z/A ratio of heavy nuclei such as ^{197}Au and ^{208}Pb for reference. They are cut off when μ_B exceeds 0.6 GeV. The trajectories are bent around the crossover temperature in Fig. 3 (a) because baryons are heavier than quarks. As the temperature decreases, the baryon chemical potential needs to increase in the hadronic phase for net baryon number conservation. The average trajectories become slightly negative in μ_Q (Fig. 3 (b)) because $\mu_n = \mu_B > \mu_p = \mu_B + \mu_Q$ in neutron-rich heavy nuclei. We observe a wide band for μ_Q, implying that a large region in the phase diagram can be explored in relativistic nuclear collisions. μ_S is

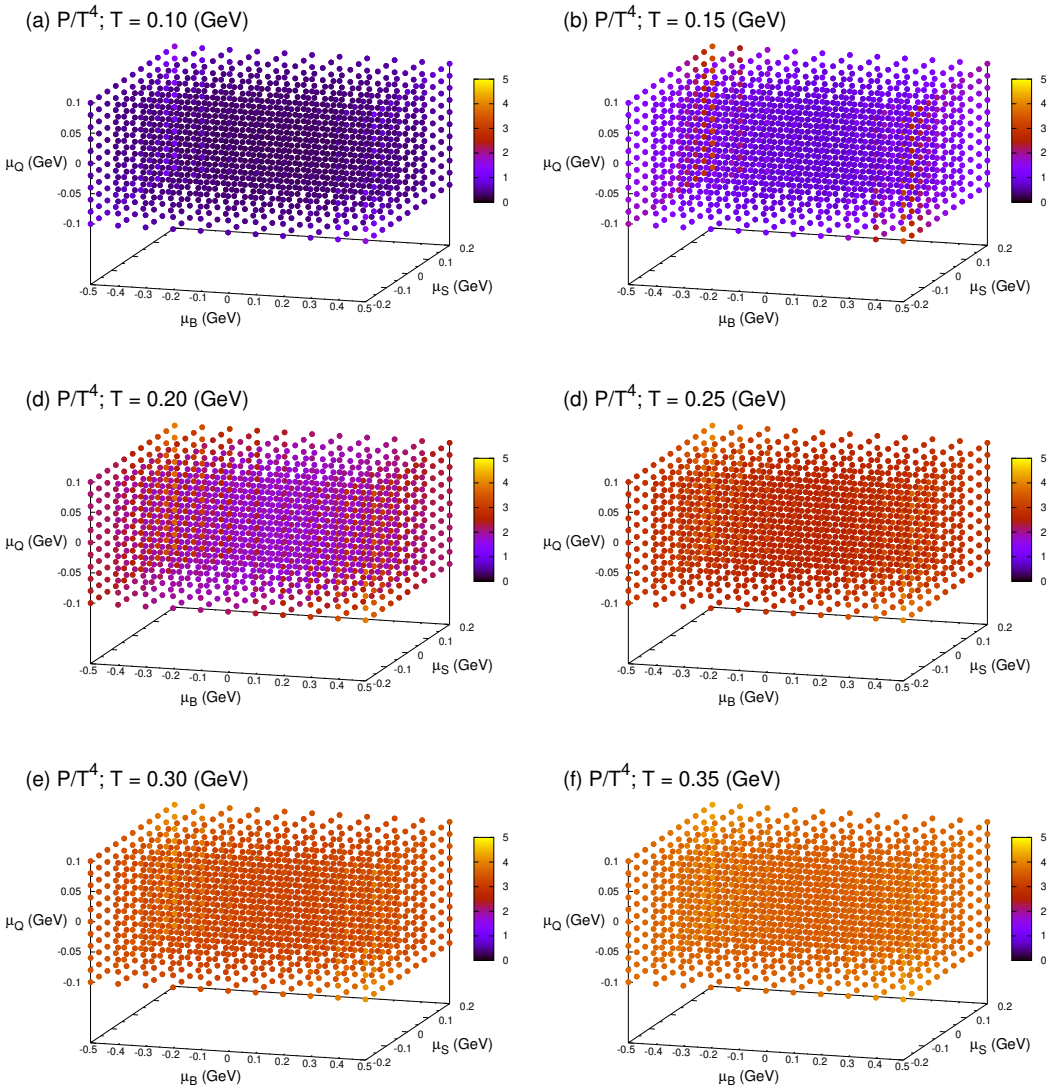

Figure 1: Dimensionless pressure P/T^4 as function of μ_B, μ_Q, and μ_S at (a) $T = 0.10$ GeV, (b) $T = 0.15$ GeV, (c) $T = 0.20$ GeV, (d) $T = 0.25$ GeV, (e) $T = 0.30$ GeV, and (f) $T = 0.35$ GeV.

finite in Fig. 3 (c) owing to the strangeness neutrality condition because the lack of strange quark chemical potential μ_s leads to $\mu_S = \frac{1}{3}\mu_B - \frac{1}{3}\mu_Q > 0$ when μ_B is positive and larger than μ_Q. The s/n_B starts to increase below $T = 0.05$ GeV, likely because the mass of kaons, which are the primary strangeness carrier there, becomes non-negligible.

Next, we develop an efficient method of application of the equation of state to the hydrodynamic model of nuclear collisions. There are 7 independent equations of motion in inviscid relativistic hydrodynamics with the three conserved charges, $\partial_\mu T^{\mu\nu} = 0$ and $\partial_\mu N^\mu_{B,Q,S} = 0$. They are expressed in terms of 8 independent variables, flow u^μ, energy density e, pressure P, and conserved charge densities $n_{B,Q,S}$. Thus, one needs the equation of state $P = P(e, n_B, n_Q, n_S)$, which characterizes the thermodynamic properties of the system, to close the set of equations. Since the pressure (2)

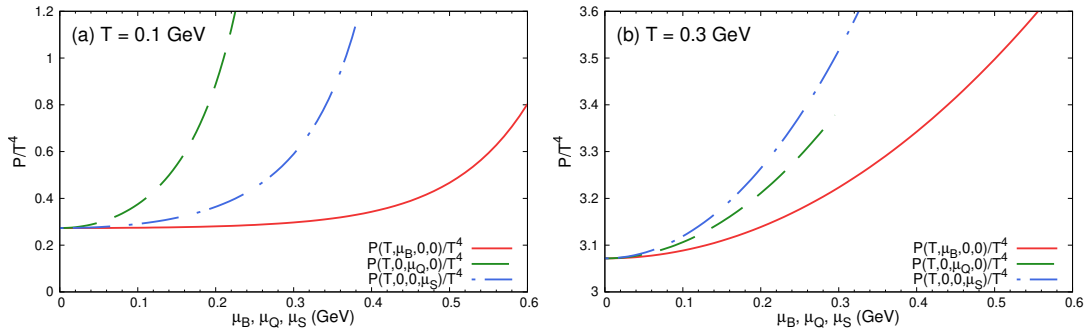

Figure 2: Dependence of dimensionless pressure P/T^4 on μ_B, μ_Q, or μ_S at (a) $T = 0.10$ GeV and (b) $T = 0.30$ GeV.

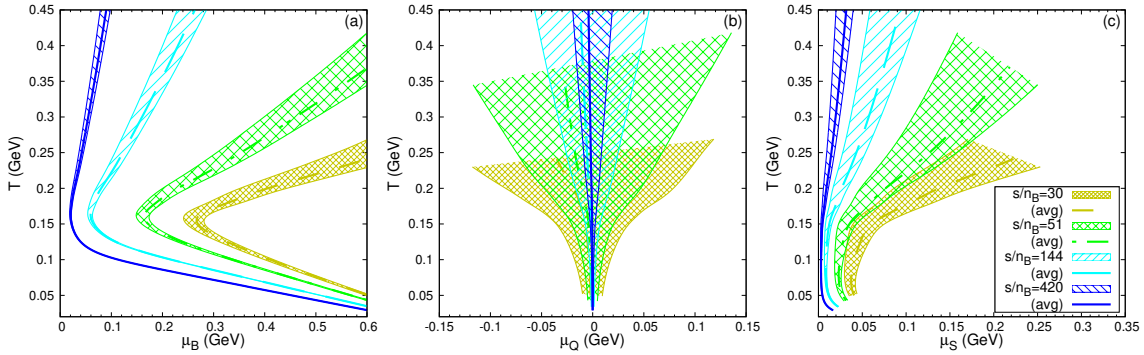

Figure 3: The regions probed when n_Q/n_B ranges from 0 to 1 for $s/n_B = 420$, 144, 51, and 30 on the (a) T-μ_B, (b) T-μ_Q, and (c) T-μ_S planes. The solid, dashed, dash-dotted, and dotted lines are the average case at $n_Q/n_B = 0.4$.

is given as a function of the conjugate variables T, μ_B, μ_Q, and μ_S, it needs to be inverted for hydrodynamic simulations. For numerical efficiency, one often prepares pre-calculated tables of the equation of state. However, the tables become too large for standard numerical implementation for a four-dimensional equation of state because e, n_B, n_Q, n_S and T, μ_B, μ_Q, μ_S have different dimensions.

We define new variables $\tilde{T}$, $\tilde{\mu}_B$, $\tilde{\mu}_Q$, and $\tilde{\mu}_S$ as the temperature and chemical potentials of the $N_f = 3$ parton gas with the same energy and conserved charge densities as our system and use them to tabulate the numerical results to overcome this issue. The parton gas equation of state is expressed as

$$e = \frac{19\pi^2}{12}\tilde{T}^4, \tag{4}$$

$$n_B = \frac{1}{3}\tilde{\mu}_B\tilde{T}^2 - \frac{1}{3}\tilde{\mu}_S\tilde{T}^2, \tag{5}$$

$$n_Q = \frac{2}{3}\tilde{\mu}_Q\tilde{T}^2 + \frac{1}{3}\tilde{\mu}_S\tilde{T}^2, \tag{6}$$

$$n_S = -\frac{1}{3}\tilde{\mu}_B\tilde{T}^2 + \frac{1}{3}\tilde{\mu}_Q\tilde{T}^2 + \tilde{\mu}_S\tilde{T}^2, \tag{7}$$

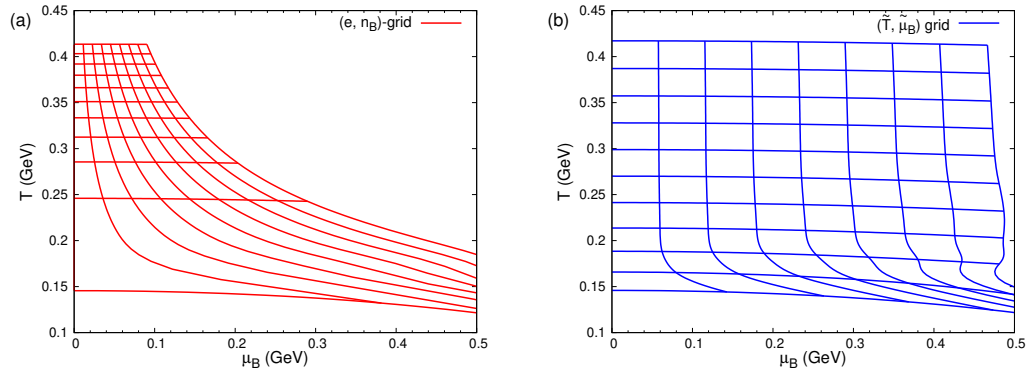

Figure 4: Comparison of grids with equal spacing in (a) e and n_B and (b) $\tilde{T}$ and $\tilde{\mu_B}$ on the T-μ_B plane.

whose solutions can be obtained analytically as

$$\tilde{T}(e, n_B, n_Q, n_S) = \left(\frac{12}{19\pi^2}e\right)^{1/4}, \tag{8}$$

$$\tilde{\mu}_B(e, n_B, n_Q, n_S) = \frac{5n_B - n_Q + 2n_S}{\tilde{T}^2}, \tag{9}$$

$$\tilde{\mu}_Q(e, n_B, n_Q, n_S) = \frac{-n_B + 2n_Q - n_S}{\tilde{T}^2}, \tag{10}$$

$$\tilde{\mu}_S(e, n_B, n_Q, n_S) = \frac{2n_B - n_Q + 2n_S}{\tilde{T}^2}. \tag{11}$$

The variables from the conservation laws can be converted into the temperature and chemical potentials of the parton gas using the relations (8)-(11), and they can be used to access the numerical results tabulated in the form of $P = P(\tilde{T}, \tilde{\mu}_B, \tilde{\mu}_Q, \tilde{\mu}_S)$. Similarly, the temperature and chemical potentials can be estimated as functions of the parton gas-based variables for particle production [34]. A successful application of the method can be found in Ref. [22].

The grids with equal spacing in (a) e and n_B and (b) $\tilde{T}$ and $\tilde{\mu_B}$ near the crossover region in the T-μ_B plane at $\mu_Q = \mu_S = 0$ are shown in Fig. 4 to illustrate the situation. One can see that the grid is deformed in the conventional e-n_B grid, leading to difficulties in covering the whole region especially in the higher dimensional cases. On the other hand, the grid is relatively uniform in the $\tilde{T}$-$\tilde{\mu_B}$ space, allowing more efficient tabulation of the equation of state for numerical hydrodynamic simulations.

4. Conclusions and outlook

We have constructed a full four-dimensional model of the QCD equation of state at finite baryon, electric charge, and strangeness densities, NEOS-4D, for hydrodynamic simulations of relativistic nuclear collisions. The pressures of the lattice QCD simulations in the Taylor expansion method and the hadron resonance gas model are matched near T_c to obtain a crossover equation of state. The other state variables can be obtained using the fundamental thermodynamic relations. The model is implemented numerically and verified to be thermodynamically consistent.

The ratio of conserved charges n_Q/n_B can vary to from 0 to 1, corresponding to neutron-rich and proton-rich regions of the initial geometry. The former may occur in the peripheral collisions of nuclei with neutron skins and the latter in proton-proton collisions. The constant s/n_B trajectories suggest that a wider region in the phase diagram can be explored in the beam energy scan programs, especially in the μ_Q direction, when the variation is taken into account.

The hydrodynamic equations of motion involve the densities e, n_B, n_Q and n_S. We have introduced the temperature and chemical potentials of a parton gas at the given energy and conserved charge densities, $\tilde{T}$, $\tilde{\mu}_B$, $\tilde{\mu}_Q$, and $\tilde{\mu}_S$, and used them to construct the tables to enable practical and efficient implementation of the equation of state. Our results serve as a pivotal component in numerical hydrodynamic simulations of nuclear collisions across various collision energies and different nuclear species. The tabulated version of the NEOS-4D results are publicly available [35].

Acknowledgments

The authors thank Frithjof Karsch, Swagato Mukherjee, and Sayantan Sharma for providing the lattice QCD data. This work is supported by JSPS KAKENHI Grant Numbers JP19K14722 and JP24K07030 (A.M.), by the U.S. Department of Energy, Office of Science, Office of Nuclear Physics, under DOE Contract No. DE-SC0012704 and within the framework of the Saturated Glue (SURGE) Topical Theory Collaboration (B.P.S.) and Award No. DE-SC0021969 (C.S. & G.P.). C.S. acknowledges a DOE Office of Science Early Career Award.

References

[1] S. Borsanyi, Z. Fodor, C. Hoelbling, S.D. Katz, S. Krieg and K.K. Szabo, *Full result for the QCD equation of state with 2+1 flavors*, *Phys. Lett. B* **730** (2014) 99 [1309.5258].

[2] HotQCD collaboration, *Equation of state in (2+1)-flavor QCD*, *Phys. Rev. D* **90** (2014) 094503 [1407.6387].

[3] HotQCD collaboration, *Equation of state and speed of sound of (2+1)-flavor QCD in strangeness-neutral matter at nonvanishing net baryon-number density*, *Phys. Rev. D* **108** (2023) 014510 [2212.09043].

[4] STAR collaboration, *An Experimental Exploration of the QCD Phase Diagram: The Search for the Critical Point and the Onset of De-confinement*, 1007.2613.

[5] P. Kolb, P. Huovinen, U.W. Heinz and H. Heiselberg, *Elliptic flow at SPS and RHIC: From kinetic transport to hydrodynamics*, *Phys. Lett. B* **500** (2001) 232 [hep-ph/0012137].

[6] B. Schenke, S. Jeon and C. Gale, *Elliptic and triangular flow in event-by-event (3+1)D viscous hydrodynamics*, *Phys. Rev. Lett.* **106** (2011) 042301 [1009.3244].

[7] P. Huovinen and P. Petreczky, *QCD Equation of State and Hadron Resonance Gas*, *Nucl. Phys. A* **837** (2010) 26 [0912.2541].

[8] J.S. Moreland and R.A. Soltz, *Hydrodynamic simulations of relativistic heavy-ion collisions with different lattice quantum chromodynamics calculations of the equation of state*, *Phys. Rev. C* **93** (2016) 044913 [1512.02189].

[9] P. Parotto, M. Bluhm, D. Mroczek, M. Nahrgang, J. Noronha-Hostler, K. Rajagopal et al., *QCD equation of state matched to lattice data and exhibiting a critical point singularity*, *Phys. Rev. C* **101** (2020) 034901 [1805.05249].

[10] A. Monnai, B. Schenke and C. Shen, *Equation of state at finite densities for QCD matter in nuclear collisions*, *Phys. Rev. C* **100** (2019) 024907 [1902.05095].

[11] J. Noronha-Hostler, P. Parotto, C. Ratti and J. Stafford, *Lattice-based equation of state at finite baryon number, electric charge and strangeness chemical potentials*, *Phys. Rev. C* **100** (2019) 064910 [1902.06723].

[12] J. Auvinen, K.J. Eskola, P. Huovinen, H. Niemi, R. Paatelainen and P. Petreczky, *Temperature dependence of η/s of strongly interacting matter: Effects of the equation of state and the parametric form of $(\eta/s)(T)$*, *Phys. Rev. C* **102** (2020) 044911 [2006.12499].

[13] A. Monnai, B. Schenke and C. Shen, *QCD Equation of State at Finite Chemical Potentials for Relativistic Nuclear Collisions*, *Int. J. Mod. Phys. A* **36** (2021) 2130007 [2101.11591].

[14] M. Kahangirwe, S.A. Bass, E. Bratkovskaya, J. Jahan, P. Moreau, P. Parotto et al., *Finite density QCD equation of state: Critical point and lattice-based T' expansion*, *Phys. Rev. D* **109** (2024) 094046 [2402.08636].

[15] C. Plumberg et al., *BSQ Conserved Charges in Relativistic Viscous Hydrodynamics solved with Smoothed Particle Hydrodynamics*, 2405.09648.

[16] A. Monnai, G. Pihan, B. Schenke and C. Shen, *Four-dimensional QCD equation of state with multiple chemical potentials*, *Phys. Rev. C* **110** (2024) 044905 [2406.11610].

[17] K. Werner, I. Karpenko, T. Pierog, M. Bleicher and K. Mikhailov, *Event-by-Event Simulation of the Three-Dimensional Hydrodynamic Evolution from Flux Tube Initial Conditions in Ultrarelativistic Heavy Ion Collisions*, *Phys. Rev. C* **82** (2010) 044904 [1004.0805].

[18] K. Aryal, C. Constantinou, R.L.S. Farias and V. Dexheimer, *High-Energy Phase Diagrams with Charge and Isospin Axes under Heavy-Ion Collision and Stellar Conditions*, *Phys. Rev. D* **102** (2020) 076016 [2004.03039].

[19] J.M. Karthein, D. Mroczek, A.R. Nava Acuna, J. Noronha-Hostler, P. Parotto, D.R.P. Price et al., *Strangeness-neutral equation of state for QCD with a critical point*, *Eur. Phys. J. Plus* **136** (2021) 621 [2103.08146].

[20] SMASH collaboration, *Particle production in a hybrid approach for a beam energy scan of Au+Au/Pb+Pb collisions between $\sqrt{s_{NN}} = 4.3$ GeV and $\sqrt{s_{NN}} = 200.0$ GeV*, *Eur. Phys. J. A* **58** (2022) 230 [2112.08724].

[21] G. Pihan, A. Monnai, B. Schenke and C. Shen, *Tracing baryon and electric charge transport in isobar collisions*, *EPJ Web Conf.* **296** (2024) 05005 [2312.12376].

[22] G. Pihan, A. Monnai, B. Schenke and C. Shen, *Unveiling Baryon Charge Carriers through Charge Stopping in Isobar Collisions*, *Phys. Rev. Lett.* **133** (2024) 182301 [2405.19439].

[23] C. Plumberg et al., *Influence of baryon number, strangeness, and electric charge fluctuations at the LHC*, in *30th International Conference on Ultrarelativstic Nucleus-Nucleus Collisions*, 12, 2023 [2312.07415].

[24] R.V. Gavai and S. Gupta, *Quark number susceptibilities, strangeness and dynamical confinement*, *Phys. Rev. D* **64** (2001) 074506 [hep-lat/0103013].

[25] C. Allton, S. Ejiri, S. Hands, O. Kaczmarek, F. Karsch, E. Laermann et al., *The QCD thermal phase transition in the presence of a small chemical potential*, *Phys. Rev. D* **66** (2002) 074507 [hep-lat/0204010].

[26] HotQCD collaboration, *Fluctuations and Correlations of net baryon number, electric charge, and strangeness: A comparison of lattice QCD results with the hadron resonance gas model*, *Phys. Rev. D* **86** (2012) 034509 [1203.0784].

[27] H.T. Ding, S. Mukherjee, H. Ohno, P. Petreczky and H.P. Schadler, *Diagonal and off-diagonal quark number susceptibilities at high temperatures*, *Phys. Rev. D* **92** (2015) 074043 [1507.06637].

[28] A. Bazavov et al., *The QCD Equation of State to $O(\mu_B^6)$ from Lattice QCD*, *Phys. Rev. D* **95** (2017) 054504 [1701.04325].

[29] S. Sharma, *private communications* .

[30] F. Karsch, B.-J. Schaefer, M. Wagner and J. Wambach, *Towards finite density QCD with Taylor expansions*, *Phys. Lett. B* **698** (2011) 256 [1009.5211].

[31] J. Cleymans, H. Oeschler, K. Redlich and S. Wheaton, *Comparison of chemical freeze-out criteria in heavy-ion collisions*, *Phys. Rev. C* **73** (2006) 034905 [hep-ph/0511094].

[32] Particle Data Group collaboration, *Review of Particle Physics*, *Phys. Rev. D* **98** (2018) 030001.

[33] J. Guenther, R. Bellwied, S. Borsanyi, Z. Fodor, S. Katz, A. Pasztor et al., *The QCD equation of state at finite density from analytical continuation*, *Nucl. Phys. A* **967** (2017) 720 [1607.02493].

[34] F. Cooper and G. Frye, *Comment on the Single Particle Distribution in the Hydrodynamic and Statistical Thermodynamic Models of Multiparticle Production*, *Phys. Rev. D* **10** (1974) 186.

[35] https://sites.google.com/view/qcdneos4d/.